学位論文

^{3}He薄膜の強磁性

東京大学大学院 理学系研究科
物理学専攻 博士課程

福島 章雄

Experimental Studies of Ferromagnetism of ^{3}He Films

A Dissertation
Presented to University of Tokyo,
in Partial Fulfillment of the Requirements for
the Degree of Doctor of Science.

by
Akio Fukushima
February,1991

Abstract

An experimental study on the coverage dependence of the ferromagnetism of ^{3}He films adsorbed on sintered silver powders is described. The static magnetization of ^{3}He films was measured for temperatures between 0.2 mK and 10 mK and for coverages from 0.10 to 0.54 atoms/Å^2 in steps of about 0.02 atoms/Å^2 and 4.5 atoms/Å^2 by a SQUID magnetometer with an external field of 4.8 mT.

The temperature dependence of the magnetization of the ^{3}He films shows that below 0.20 atoms/Å^2 the magnetization well obeys the Curie law and above that a ferromagnetic contribution appears. The isotherm of the magnetization at 0.2 mK has four peaks at coverages of 0.23, 0.29, 0.35, and 0.41 atoms/Å^2.

The Curie constant of the ^{3}He film is deduced from the temperature dependence of the magnetization above 2 mK. The Curie constant increases in proportion to the coverage up to 0.20 atoms/Å^2, and becomes almost constant above that value, which is that of the free spin of 0.24 ± 0.04 atoms/Å^2. Below 0.20 atoms/Å^2 the Curie constant is smaller than the free spin value. This suggests the coexistence of liquid and solid in the second layer. The coverage dependence of Curie constant shows that the second layer solidifies completely at 0.20 atoms/Å^2 and ^{3}He atoms above the second layer behave as liquid.

The exchange constant is deduced from the magnetization on the following assumptions: Only the second layer contributes to the ferromagnetism; Curie constant of the second layer above 0.20 atoms/Å^2 is unchanged when more ^{3}He are put on the second layer. Exchange constant begins to appear above 0.20 atoms/Å^2 and increases as the coverage increases. Moreover, it has four peaks at 0.23, 0.29, 0.35, and 0.41 atoms/Å^2. These peaks appear with the same interval of 0.06 atoms/Å^2, which is nearly equal to the areal density of one liquid layer. The multipeak structure of the exchange constant implies that the exchange interaction in the ^{3}He film is dependent on the number of liquid layers.

Acknowledgments

This study was performed in the ULT (Ultra-Low Temperature) group of I. S. S. P. over the years 1986 to 1990. The study was achieved with the contributions of almost everyone in the ULT and the cryogenic service station. I feel very fortunate to have been able to study in the ULT group. This laboratory has truly been comfortable for me, and is very active in the physics field.

The work has been closely supervised by Prof. Yuichi Okuda, who has taken an active part at all stages of this study. I wish to thank him for the support and guidance I have received during these six years. I am also grateful to him for constructive criticism on all my manuscripts, of course including this thesis. I sincerely thank Prof. Shinji Ogawa, the chief of ULT, for his continuous encouragement and indispensable support. I also extend thanks to Dr. H. Fukuyama, who contributed to my understanding of the ^{3}He films, and to Mr. T. Kawae, who helped me in improving the experimental apparatus.

It was one of most pleasurable experiences to visit the low temperature laboratory of C. N. R. S. In particular, I would like to acknowledge Prof. H. Godfrin for valuable suggestions and discussions about this study.

Finally, I note that this work was partly made possible by my being awarded by a Fellowships of the Japan Society for the Promotion of Science for Japanese Junior Scientists.

Tokyo, February 1991

Akio Fukushima

Contents

1. Introduction

This thesis presents the results of experimental studies on the ferromagnetism of ^{3}He films adsorbed on sintered silver substrate.

The surface induced ferromagnetism of liquid ^{3}He was first observed in contact with Mylar sheets [1], and thereafter many experiments were done with various kinds of substrates such as Vycor glass, graphite and sintered silver powder. The magnetization of liquid ^{3}He shows a common Curie-Weiss temperature θ of the order of 0.5 mK for most substrates [2]. Such a large ferromagnetism does not appear in bulk solid or liquid ^{3}He. The coverage dependence of the magnetization without bulk liquid was studied to learn the mechanism of the ferromagnetism, and the results revealed that the ferromagnetism has its origin in the second solid layer.

From a geometrical point of view, the ^{3}He film has 2D configuration, and is expected to be an ideal 2D Heisenberg system. The mechanism of the ferromagnetism, however, has not yet been clarified. Two types of theoretical interpretations are proposed: one is a three particle ring exchange in the second layer; the other is an indirect exchange between the solid atoms mediated by liquid layers.

The purpose of this study was to identify the origin of the ferromagnetism from the magnetization measurement. Using sintered silver substrate we intended to cool the ^{3}He films as much as possible. We expected that the temperature dependence and the coverage dependence of the magnetization would provide information about the character of the ^{3}He film system and the mechanism of the surface induced ferromagnetism.

1.1 Phase Diagram of ^{3}He Films on Graphite

^{3}He atoms are adsorbed on a substrate by the Van der Waals potential at low temperatures. As the Van der Waals potential of the substrate decreases as z^{-3}, where z is the distance from the surface, the density of each adsorbed layer changes as a function of z. Numerical calculation of the density profile of the ^{3}He film was done by the Van der Waals potential and continuous fluid approximation [3]. The calculation shows that the density of the first layer is as large as that of bulk solid ^{3}He at several hundred bars, and the density of the second layer is as large as that of bulk ^{3}He at several tens of bars. Determination of the phase of the second layer cannot be made by the calculation as the melting pressure of solid ^{3}He is 34 bars.

The phase diagram of ^{3}He films adsorbed on graphite has been drawn by heat capacity measurements. The heat capacity of the ^{3}He film has peaks corresponding to solidifications in the first and second layers around 1 K. Figure 1.1 shows the phase diagram. The phases are identified by the recent heat capacity measurement from 200 mK down to 2.5 mK [4]. Each adsorbed ^{3}He layer is shown to exist as a liquid, as a solid registered to the substrate, or as an incommensurate solid depending on its density.

For low temperatures the phase of the ^{3}He film is stable and determined solely by the areal density. Below 10 mK, the first layer solidifies at 0.06 atoms/Å^2, and the second layer solidifies at 0.18 atoms/Å^2. Promoted atoms on these layers compress the first layer by a few percent but the second layer by 20 %. The layers above the second layer do not solidify. The numerical calculation shows that the density of the adsorbed layer does not greatly change above the second layer, and is almost equal to that of the bulk liquid.

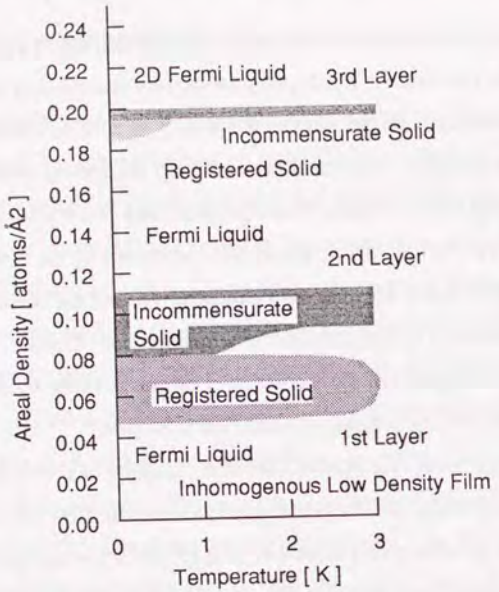

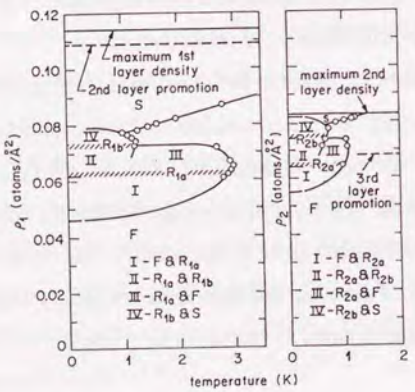

Figure 1.1 Phase diagram of ^{3}He film adsorbed on graphite. Above: rough sketch of the structure of the ^{3}He film. Below: detailed phase diagram [4].

1.2 Ferromagnetism of ^{3}He Films

Experimental studies for the coverage dependence of magnetization, heat capacity and neutron diffractions were done to identify the origin of the ferromagnetism. Graphite and sintered silver powder were used as substrates.

The graphite is considered an ideal substrate having a flat surface and a large surface area per unit volume. ^{3}He film adsorbed on the graphite is expected to be an ideal 2D Heisenberg system. On the contrary, the sintered silver powder has good thermal conductivity, and therefore can easily cool the ^{3}He film to an ultralow temperature. Although the surface of the sintered silver powder is not characterized as well as the graphite, we consider that the surface is sufficiently homogeneous to be able to compare the results with that of the experiments done for graphite substrate.

From an experimental point of view, a study of surface induced ferromagnetism on the sintered silver is important. The sintered silver powder is used widely as a heat exchanger in low temperature experiments, such as those on liquid ^{3}He, solid ^{3}He, ^{3}He–^{4}He mixture, etc. Surface induced ferromagnetism is a serious problem for these magnetization measurements.

1.2.1 Results on Graphite

The experimental results done for the ^{3}He films adsorbed on the graphite substrate are summarized in this section. Figure 1.2 shows the results of magnetization, neutron diffraction, and heat capacity measurements.

The NMR measurement observed a large peak at 0.24 atoms/Å^2 in the isotherm of the magnetization at 3 mK [5]. The isotherms of the magnetization of the ^{3}He film are shown in the upper graph of Fig. 1.2. The temperature dependence of the magnetization at 0.24 atoms/Å^2 is described well by the 2D Heisenberg model with an exchange constant $J = 2.1$ mK for temperature down

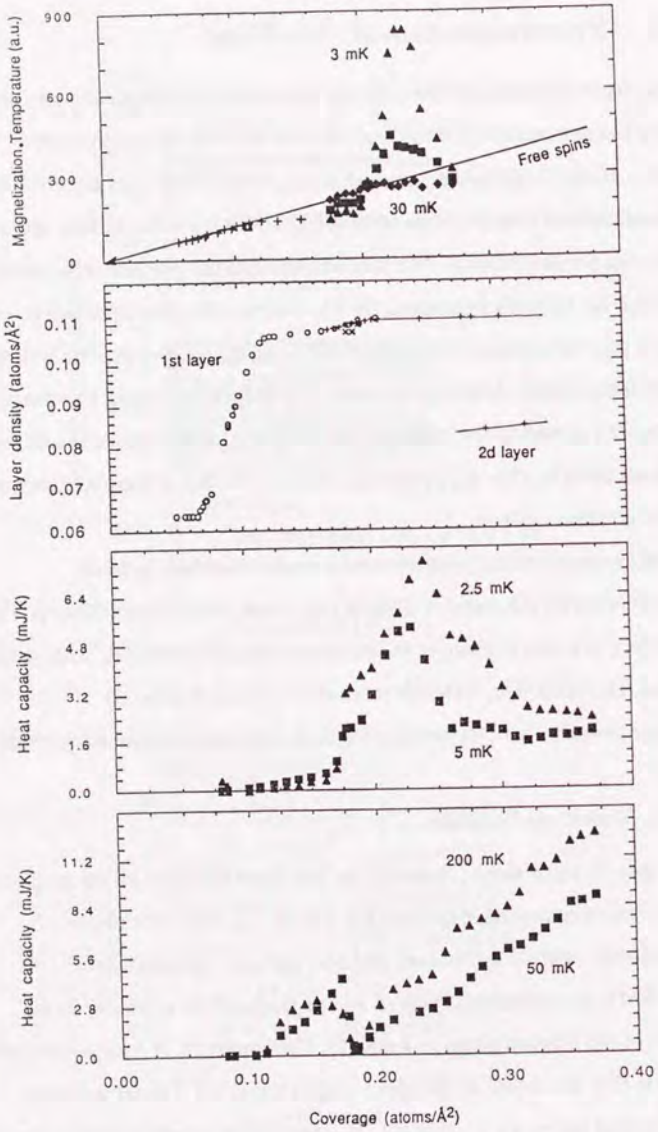

Figure 1.2 Results of various measurements done for ^{3}He films adsorbed on graphite. Magnetization [5], neutron diffraction [7,8], heat capacity for lower and higher temperatures [4] are represented. This graph was prepared by H. Godfrin.

to 2 mK [6]. At the lowest temperature of 0.4 mK the magnetization amounts to about 80 % of the saturation magnetization.

A neutron diffraction experiment can determine whether an adsorbed ^{3}He layer solidifies or not. At 0.133 atoms/Å^2 one diffraction peak of the first layer is observed, and at 0.297 atoms/Å^2 two diffraction peaks of the first and the second layers are observed [7]. The coverage dependence of the density of the adsorbed layers is also determined by neutron experiments [8]. The result is shown in the next upper graph of Fig. 1.2. The figure shows that the density of the first adsorbed layer increases by promoted atoms on the first layer, and the first layer is completed at 0.108 atoms/Å^2.

The lower two graphs in Fig. 1.2 show the isotherms of heat capacity of the ^{3}He film adsorbed on graphite [4]. Small heat capacities at 200 mK at the coverage of 0.06 atoms/Å^2 and 0.186 atoms/Å^2 indicate solidifications of the first and the second layer respectively. Below 5 mK the nuclear spin contribution appears above 0.186 atoms/Å^2. At 2.5 mK a large peak of the heat capacity is observed at 0.23 atoms/Å^2. Above 0.23 atoms/Å^2 the heat capacity decreases as the coverage increases.

1.2.2 Results on Sintered Silver

Figure 1.3 shows the results of magnetization and heat capacity measurements of ^{3}He films adsorbed on sintered silver powder.

The static magnetization was measured by a SQUID magnetometer [9] for temperatures between 0.8 and 10 mK and for coverages from 0.5 layers up to bulk liquid of a saturated vapor pressure with an external field of 48 mT. The temperature dependence of the magnetization shows that the ferromagnetic tendency varies as a function of the coverage. The upper two graphs of Fig. 1.3 show the coverage dependence of the Curie constant and the Weiss temperature of the ^{3}He films. The Curie constant increases in proportion to the coverage up

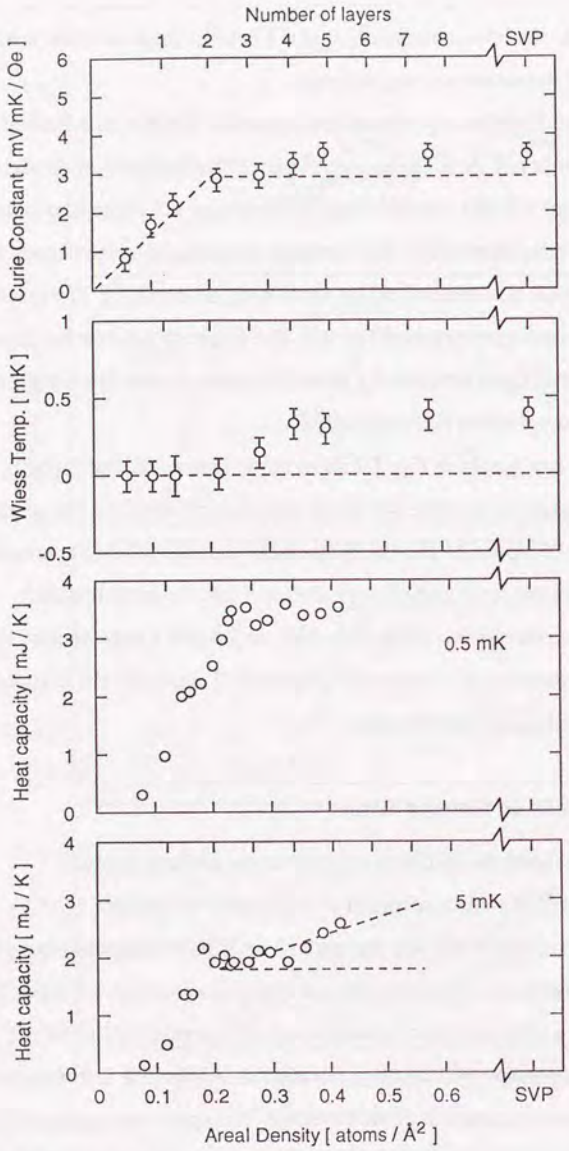

Figure 1.3 Results of magnetization [9] and heat capacity measurement [10] done for ^{3}He films adsorbed on sintered silver substrate.

to 0.2 atoms/Å^2, and becomes almost constant above that, while the Weiss temperature increases from 0 to 0.4 mK as the coverage increases between 0.2 and 0.4 atoms/Å^2, and becomes constant above 0.4 atoms/Å^2. These results show that adsorbed layers above the second layer behave as degenerated Fermi liquid, and the ferromagnetism appears after the liquid layer is formed.

The heat capacity of the ^{3}He film adsorbed on sintered silver powder was measured for temperatures between 0.4 and 7 mK and for coverages from 0.8 to 5 layers [10]. The isotherms of the heat capacity are shown in the lower two graphs in Fig. 1.3. The isotherm of the heat capacity below 1 mK has two peaks at 0.24 and 0.32 atoms/Å^2. A fit of the heat capacity at 0.24 atoms/Å^2 to the 2D Heisenberg ferromagnet with triangular lattice gives the exchange constant $J / k_B = 0.17$ mK. The same fitting of the heat capacity at 0.4 atoms/Å^2 gives $J / k_B = 0.14$ mK. The magnitude of these exchange constants agrees well with the Weiss temperature θ deduced from the magnetization measurement. The relation between J / k_B and θ is $J / k_B = \theta/3$.

After spin contributions ($\propto 1/T^2$) and a Fermi degenerated liquid contribution ($\propto T$) are subtracted, a large heat capacity remains above 0.16 atoms/Å^2. This large heat capacity seems to be independent of the temperature between 0.4 and 7 mK and also independent of the coverage. If it is from the second layer atoms, it corresponds to $0.2N_2k_B$ where N_2 is the number of atoms in the second layer.

1.3 Theories for Ferromagnetism of ^{3}He Film

Some theoretical interpretations have been proposed for the surface induced ferromagnetism, such as a three particle ring exchange process in the second layer, and an indirect exchange process via a bulk liquid ^{3}He or 2D Fermi liquid ^{3}He. In this section we briefly review these theories.

1.3.1 Current Theories for Surface Ferromagnetism

Several exchange models have been proposed to account for the origin of the surface induced ferromagnetism. Considering the experimental results, two types of exchange mechanisms seem promising: a cyclic 3 spin exchange model in the solid layer, and an indirect exchange via liquid atoms.

The cyclic 3 spin exchange was proposed by Roger and Delrieu [11]. This theory is based on the steric argument that a hard core potential of ^{3}He atom favors three particle exchange rather than two or four particle exchange in 2D or 3D triangular geometry. This mechanism predicts the ferromagnetism in hcp solid ^{3}He, which has been studied experimentally for some years [12]. The exchange constant strongly depends on the density of the solid layer. The derivative $\partial \ln J / \partial \ln d$, where d is the interatomic distance in 2D solid, is estimated to be 20 ± 3 [11]. Figure 1.4 shows the relation between J / k_B and d. Since the density of the first layer is extremely high, the exchange interaction in this layer is estimated to be of the order of 1 μ K. Using the density of the solid second layer of 0.077 atoms/Å^2, the theory gives the exchange interaction of the order of 1 mK.

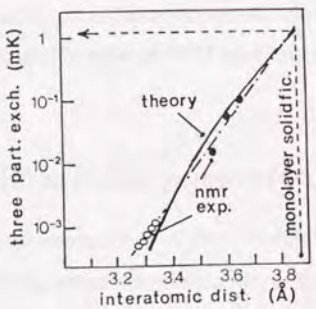

Figure 1.4 Three particle exchange in 2D solid ^{3}He [11]. The solid curve corresponds to the theoretical predictions. Arrow indicates the expected exchange interaction from the solid second layer.

An indirect exchange interaction between adsorbed solid atoms via liquid atoms was first proposed by Jichu and Kuroda [13]. They modeled the system as the 2D solid layer and the bulk Fermi liquid, and proposed two types of indirect exchange processes: indirect exchange between two atoms in the solid layer mediated by the liquid atom (RKKY type interaction, ferromagnetic), and two particle exchange via hole state in the liquid (antiferromagnetic). Using a simplified model and a second order perturbation theory, they showed the indirect exchange via liquid atoms is dominant. This theory gives the same order of exchange interaction as observed experimentally.

An indirect exchange process which has explicitly taken the coverage dependence into consideration was proposed by Guyer [14]. In this theory, the adsorbed ^{3}He film is modeled as 2D solid interacting with 2D Fermi liquid. The liquid layer is regarded as a system of fermions in an adjustable box which has the discrete perpendicular energy states labeled by integer m. The z part of the wave function of the solid layer sticks out into the liquid layer. The overlap integral between the wave function of liquid layer and that of solid layer leads to m dependence of the RKKY interaction.

The RKKY interaction results from a particle at site R of spin σ in the solid layer (R, σ) making a transition to the empty state (q', σ) in the liquid layer with a particle from an occupied state in the liquid layer (q, σ') going to (R, σ'). The further transition (S, σ'') $\rightarrow$ (q , σ''), (q', σ) $\rightarrow$ (S, σ) leads to an exchange of the spins (σ, σ'') among the solid layer sites (R, S). This process results in a three particle exchange. Figure 1.5 illustrates the exchange process.

Figure 1.6 shows the result of the numerical calculation of $K(R,S)$ vs d [14]. The process consists of interactions of the solid layer with atoms in excited state and hole state of the liquid layer. Assuming the process is caused by the states in the same energy level m, the exchange constant oscillates as a function of liquid thickness, and has peaks at the half-filled state of each liquid layer.

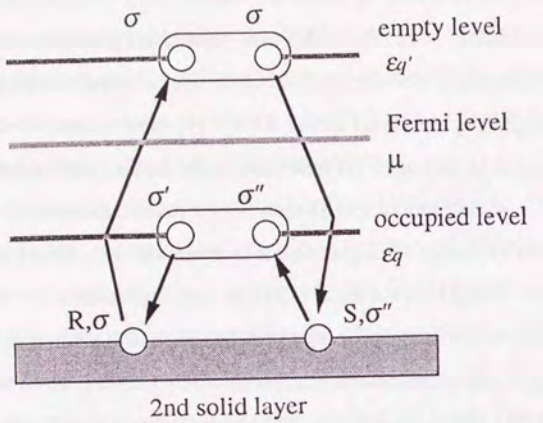

Figure 1.5 Exchange process of the indirect exchange process via 2D degenerated liquid layer. This process is equivalent to the 3 particle exchange process.

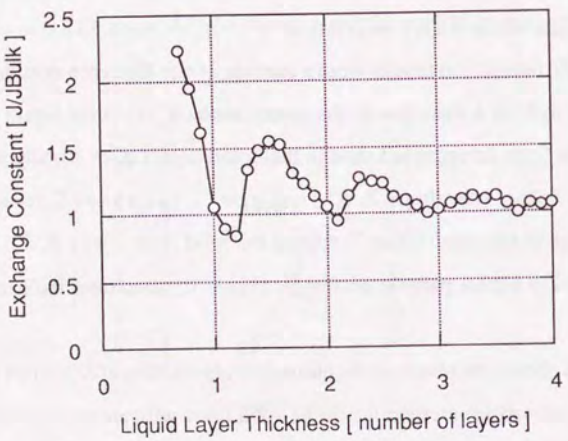

Figure 1.6 Coverage dependence of the exchange constant [14]. The constant has peaks at about integer and half number of liquid layers.

1.3.2 2D Heisenberg Ferromagnet

Considering the configuration of the ^{3}He film, the ferromagnetic interaction is expected to be represented by the nearest neighbor 2D Heisenberg model, of which Hamiltonian is

$$H = -J \sum_{i,j} \boldsymbol{\sigma}_i \cdot \boldsymbol{\sigma}_j .$$

For the triangular lattice, the susceptibility and the specific heat was calculated by the high temperature series expansion [15]. The susceptibility is given by

$$\chi(T) = \frac{C}{T}\left(1 + 3X + 6X^2 + \frac{17}{2}X^3 + \ldots\right),$$

where $C = \dfrac{Ng^2\mu_N^2 I(I+1)}{3k_B}$ and $X = \dfrac{J}{k_B T}$,

and the heat capacity is given by

$$C(T) = N k_B \left(\frac{9}{4}X^2 + \frac{18}{8}X^3 + \ldots\right).$$

Another feature of this system is that the spontaneous magnetization does not appear even at $T=0$. The proof was given by Mermin-Wagner [16] using the Bogolyubov inequality.

2. Experimental

2.1 Adiabatic Nuclear Demagnetization Apparatus

A powerful refrigerator is indispensable for the study of the ferromagnetism of ^{3}He films adsorbed on sintered silver powder, as the Curie-Weiss temperature θ is of the order of 0.5 mK. In this section we describe the nuclear refrigerant, the thermometer and the magnetization cells.

2.1.1 Nuclear Refrigerant

The nuclear stage was made of a massive copper rod [17]. The copper material was a standard, commercial, tough-pitch copper with purity of 99.96 %. The residual resistance ratio R_{300K}/R_{4K} of a sample piece of the same material with the same heat treatment was 550 ± 50. The central part of the stage was fixed in the center region of a 7 Tesla superconducting solenoid. The effective mass of the nuclear stage is 37 moles.

The heat switch was made of an aluminum rod of 10 mm diameter with purity of 99.999%. Two contacts were welded by an electron beam to pure silver rods. The aluminum part was machined to make 3 slits across both welded contacts to reduce the phonon mean free path and eddy current heating during the field sweep.

The magnetized nuclear stage was precooled by a conventional dilution refrigerator [18] down to 18 mK. All demagnetization procedures were controlled by a personal computer [19] using a GP-IB interface. The bundle was demagnetized from 6.5 T to 9 mT following the function $B=B_0 \exp[-\tau / t]$, where B_0 is an initial field and τ is a time constant which

was chosen to be 240 minutes. The nuclear stage reached the lowest temperature below 0.2 mK 24 hours after the demagnetization started.

The heat-leak was estimated from the warming up rate of the nuclear stage. An unknown time dependent heat-leak was observed. At the first demagnetization the heat-leak was 1.5 nW. After 30 days from the initial cooling the heat-leak decreased to 0.5 nW and became constant [17]. We found that the heat-leak also depended on the thickness of the ^{3}He film. In the case of an empty cell or with ^{3}He film below 0.20 atoms/Å^2, the heat-leak was about 0.5 nW. For higher coverages, the heat-leak became 0.8 nW at 0.35 atoms/Å^2, and 1 nW at 4.5 atoms/Å^2.

Figure 2.1 shows an overview of the nuclear demagnetization apparatus. The experimental space was constructed by two flanges of 80 mm diameter and three rigid silver rods of 14 mm diameter. The vertical length of the experimental space is 220 mm. The silver rods play a role as thermal links and support members of the nuclear stage.

Experimental cells were attached to both flanges. A superconducting fixed points device was placed on the upper flange. The NMR (Nuclear Magnetic Resonance) thermometer and the magnetization measurement cells were placed on the lower flange which was bolted to the top flange of the nuclear stage.

2.1.2 Thermometer

A platinum pulsed NMR was used as a thermometer for these temperature region [20]. The sensor was made of 10^4 platinum wires of 20 μm diameter. One end of the wires was welded to a platinum plate by TIG (Tungsten Inert Gas) welding. Then the platinum plate was attached to a silver rod by four 3 mm screws. A conventional single coil method was adapted with the operating frequency of 250 kHz. The basic electric circuit was made in this laboratory. We refined the preamplifier and the digital circuit, and added a GP-IB interface

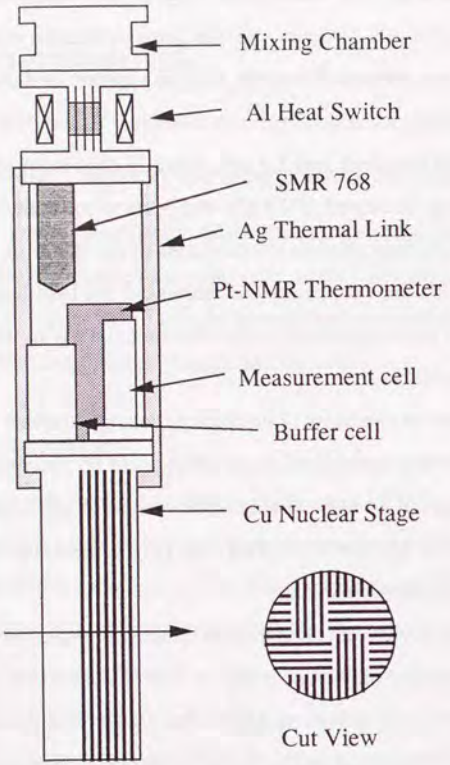

Figure 2.1 An overview of the nuclear refrigerant. The drawing shows the main part used in this experiment, except the wiring of the thermometer and capillaries of the experimental cells.

in the course of this experiment. This thermometer was also controlled by the computer, which rectified the pulse, changed the interval between the pulses and the gain, and transferred the data to the computer. The interval of the pulse τ was determined by the function $\tau=300/T$ second, where T is in mK. The constant value of 300 means that τ is 10 times as long as the T_1 of the platinum nucleus.

Since the NMR thermometer is a secondary thermometer, the calibration must be done by another standard thermometer. In this experiment the NMR thermometer was calibrated by a superconducting fixed points device [21]. To prevent the problem of supercooling, the transition must be measured in the warming up process. For our NMR thermometer two transitions were used, 23.15 mK of beryllium and 15.6 mK of tungsten. We calibrated the NMR signal by both transitions 5 or 6 times while warming the nuclear stage slowly. The temperature was increased by PID (Proportional Integral Differential) feedback method with the sweep rate of 0.05 mK/min. The coefficients of the relation to convert NMR signal to the temperature were determined within 1 % accuracy.

2.1.3 Experimental Cells

We prepared two different experimental cells, one the magnetization measurement cell and the other the buffer cell. A cut view of both cells is shown in Figure 2.2. The bodies of both cells were machined from a silver rod of 99.99 % purity, and annealed at 650 °C for 24 hours to obtain good thermal conductivity [22]. The fine silver powder for substrate was made from pure pulverized silver shots of 99.999 % purity [23].

The magnetization cell was designed to cancel the magnetization of the sintered silver as much as possible. A pick-up coil formed the first order gradiometer. The cell body has two separated cavities and two slits around the body for the pick-up coil. One side is for the magnetization of only sintered silver and the other is for that with the ^{3}He film. Using an astatic coil with 8 turns for each side, only the magnetization of the ^{3}He film can be detected.

For both sides the same amount of fine powder was sintered under the same conditions. The mass of the silver powder was 5.15 g per side. First, presintered powder was compressed tightly in a layer 1 mm thick at the bottom of each

side. The presintered powder was made by heating it at 200 °C for 20 minutes in 3 Torr of H_2 gas. Furthermore, normal fine powder was packed on top of the 1 mm thick layer to a packing factor of 44 % several times until the whole cavity was filled with silver powder. Using a Teflon jig to keep the powder under pressure, the cell was heated at 130 °C for 5 min. After sintering, each side was closed by silver caps with capillaries and sealed by a few drops of stycast 1266. The reference side was pumped to vacuum to avoid contamination by water, oxygen, and sulfur oxides in the air, and sealed at room temperature. The surface area of the ^{3}He film side after the sintering was 8.94 m^2. The method measuring surface area is described in section 2.2.

A superconducting solenoid coil was designed for placement just outside of the magnetization cell. This solenoid produced a static field of 4.8 mT with a current of 40 mA. To prevent noise and fluctuations of the current source, the magnetic field was applied in persistent mode. A niobium tube used as a magnetic shield was 2 mm thick, 30 mm in inner diameter and 100 mm long. The entire magnetization cell was protected by this shield.

The buffer cell was designed to have a surface area about 10 times that of the magnetization cell to stabilize the ^{3}He film thickness and to be able to control the coverage more precisely. Material for this cell was the same as that used in the magnetization cell. To maintain good thermal contact with the ^{3}He films, this cell has a 5 mm diameter rod in the center of the cavity. The fine silver powder was packed around the rod and compressed to a packing factor of 46 %. Then this cell was heated at 150 °C for 30 min. in vacuum and gradually cooled down. The total mass of silver powder is 100.3 gr and the surface area after sintering is 108.3 m^2.

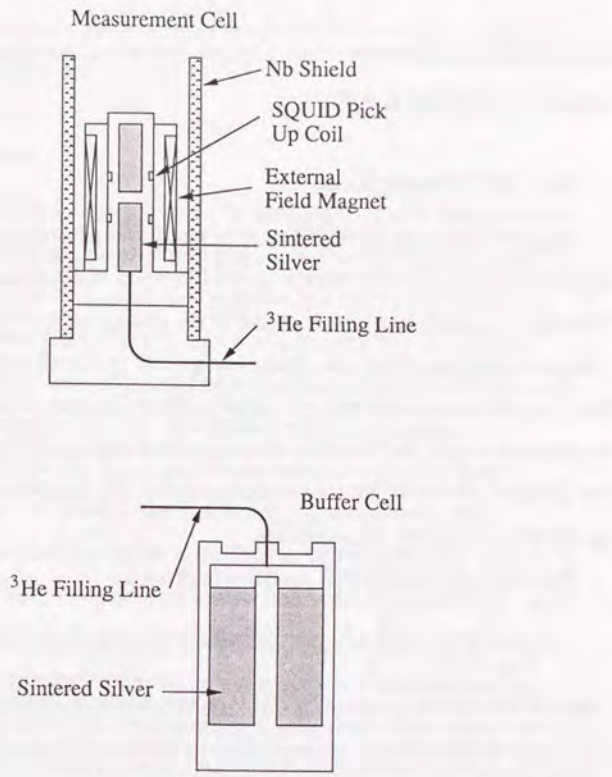

Figure 2.2 Cut views of the experimental cells. Both cells are made of pure silver. A tubing of 0.6 mm outer diameter and 0.2 mm inner diameter was used for the ^{3}He inlet capillary.

2.2 Surface Area Measurement

The surface area of the sample cells was determined using the vapor pressure isotherms of adsorbed nitrogen and argon at 77.3 K. These isotherms were analyzed by BET (Brunauer-Emmett-Teller) theory [24]. In this section we begin with a discussion of the BET equation. We then describe the apparatus

used in surface area measurement, and compare the results deduced from the isotherms of nitrogen and argon.

2.2.1 BET Measurement

Since the advent of the BET theory of multilayer adsorption, adsorption isotherm measurement has been a common method of determining surface area. The theory is based on a kinetic model of the adsorption process put forward by Langmuir and simplified with some assumptions: that in all layers except the first layer the heat of adsorption is equal to the molar heat of condensation; that in all layers except the first layer the evaporation and condensation conditions are identical; that at the saturation vapor pressure P_0, the adsorptive condensation to a bulk liquid occurs.

Thus, the well-known BET equation is given by

$$\frac{X}{V_{ads}\,(1-X)} = \frac{1}{V_m} + \frac{C-1}{V_m\,C}X\ ,$$

where X is a relative pressure P/P_0, V_{ads} is volume of adsorbed gas, and V_m is volume of adsorbed gas corresponding to monolayer completion. C is the parameter concerned with the difference of the heat of adsorption between the first layer and the liquid layers.

The most suitable region, which is called the BET regime, of the adsorption isotherm lies from $0.05X$ to $0.30X$. This is a fairly flat region of the isotherm where multilayer adsorption begins. Under $0.05X$ an initial adsorption occurs in micropores having diameters less than 20 Å, so that the BET equation cannot be applied. This area is characterized by the condition of the surface. Although many studies have been done in this region, it has been very difficult to determine the roughness or the micropore distribution.

If a capillary condensation occurs on the surface, hysteresis appears between the adsorption and the desorption isotherm. Since no hysteresis on the isotherm

was observed, we consider the surface of the sintered silver is homogeneous enough on the atomic scale.

2.2.2 Apparatus

We fabricated a convenient apparatus for precision isotherm measurement which was designed to decrease the free space in the sample space as much as possible. Use of two methods made this possible: one was to decrease the physical volume using small size capillaries, and burying free space in the sample cell and the pressure gauge; the other was to decrease the effective free space using the adsorption gas with lower saturated vapor pressure.

We adopted nitrogen and argon gas for the adsorption gas and liquid nitrogen for coolant. At 77.3K of the liquid nitrogen temperature, both saturation vapor pressures are rather high. Thus to decrease the free space to the greatest extent possible, we made a new apparatus with a very small free space of 0.2 cc except for the void space in the sintered silver powder. Moreover, to determine the free space in the sintered silver exactly, we measured the free space using ^{4}He gas at 77.3 K, a temperature at which no condensation occurs.

Figure 2.3 illustrates the apparatus. The entire gas handling system including the pressure gauge, the valves, the standard volume, and the tubing, was placed in the box whose temperature was controlled by a PID temperature controller within ± 0.1 °C. The valves were manipulated through long shafts in order not to disturb the temperature inside the box.

A barocell type pressure gauge of 100 Torr full scale [25] was used for the argon isotherm measurement, and a setra pressure gauge of 1.7 bars full scale [26] was used for nitrogen isotherm measurement. These capacitance pressure gauges have quick response and fairly high resolution and stability, making them ideal for isotherm measurements.

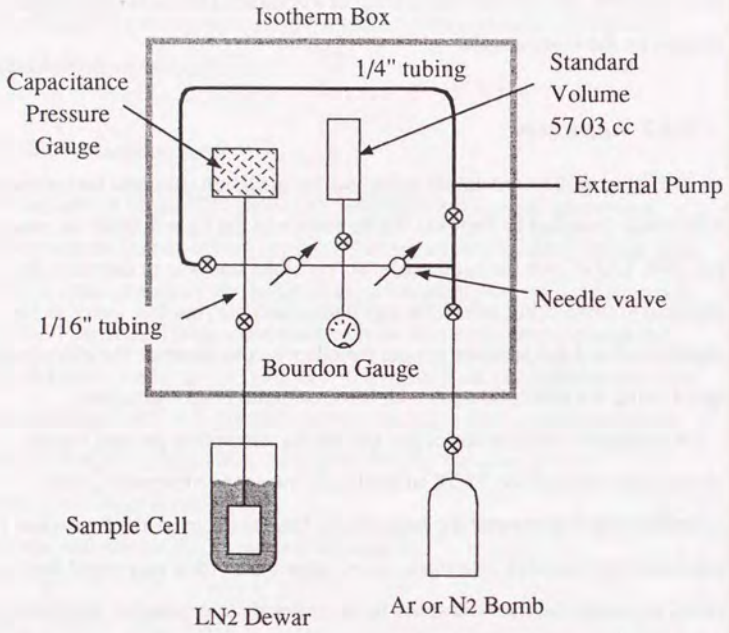

Figure 2.3 Block diagram of the BET measurement apparatus. The isotherm box was controlled by a PID temperature controller within ± 0.1 °C. The liquid nitrogen dewar is placed just beneath the isotherm box.

2.2.3 Measurement of Experimental Cells

The surface area of the magnetization cell was measured by nitrogen and argon gas. We adopted 760 Torr for the saturated vapor pressure of nitrogen and 233 Torr for that of argon at 77.3 K. Figure 2.4 shows the adsorption isotherms of both gases. The BET analysis of the nitrogen isotherm gives the surface area of 8.94 ± 0.03 m^2 using the standard surface area per molecule of 16.2 $Å^2$. The analysis of the argon isotherm gives the surface area of 9.21 ± 0.16 m^2 using the standard surface area per molecule of 16.65 $Å^2$. The surface area of the buffer cell was measured by nitrogen alone. Figure 2.5 shows the adsorption isotherm for the buffer cell. The BET analysis gives the surface area of 108.3 ± 0.9 m^2.

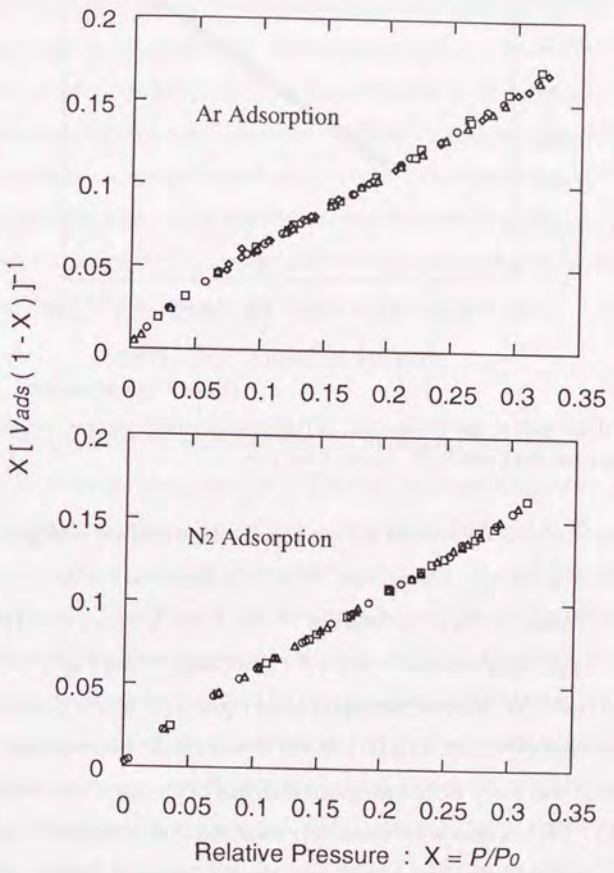

Figure 2.4 BET plot of the magnetization cell. The adsorptions isotherm of argon and nitrogen gas were measured, and the argon isotherm was found to be much scattered.

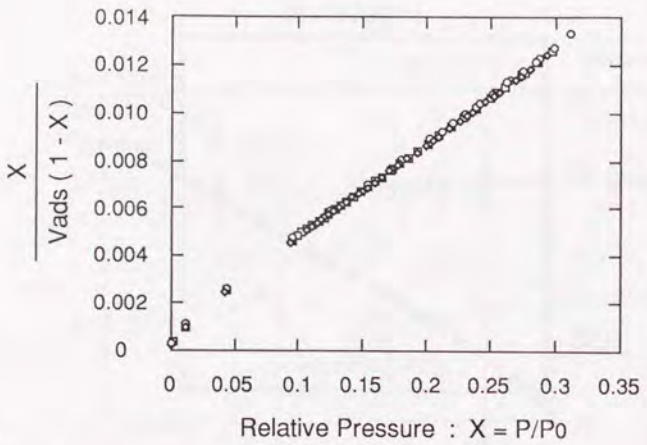

Figure 2.5 BET plot of the buffer cell. In this measurement we focused the isotherm between $0.1X$ and $0.3X$, where $X = P / P_0$.

The argon isotherm is expected to have an advantage over the nitrogen isotherm, because argon is monoatomic, chemically inert, and has no quadrupole moment. As the temperature of 77.3 K is below the tricritical point of argon, it cannot be determined whether the adsorbed layers are solid or supercooled liquid. We adopted the supercooled liquid state which gives more natural adsorption curves up to P_0 [27]. In our measurement, however, the argon isotherm was much more ambiguous than that of nitrogen. The nitrogen isotherm at 77.3 K has been most commonly used due to the availability of gas and liquid nitrogen. It compares broadly with the data acquired, and has greater reproducibility. Thus we used the surface area from the nitrogen isotherm for the experiment.

2.3 Magnetization Measurement

The magnetization was measured in a static field using a SQUID (Superconducting QUantum Interference Device) magnetometer [28]. The

SQUID magnetometer has very high sensitivity, but also has problems in that it cannot determine the absolute zero magnetization and there are many breakpoints in output voltage. Due to the breakpoints the output voltage must be connected to get the magnetization. As the magnetization of sintered silver substrate was not cancelled completely, the difference of the magnetization with and without the ^{3}He film was determined to obtain the magnetization of the ^{3}He film. The unbalanced magnetization of the sintered silver substrate was observed as the background magnetization, which was well explained by a free spin model with three different magnitudes of magnetic moments. In this section we describe the details of the magnetization measurement.

2.3.1 Measurement Circuit

The pick-up coil of the magnetization cell formed the first order gradiometer. Only the magnetization of ^{3}He film was transferred to the SQUID element by superconducting twisted pair covered with lead tubing. Figure 2.6 shows a systematic diagram of the measurement circuit. The SQUID element was placed on the 1K plate with stainless supports, and was anchored weakly to the 1K plate. Its temperature was controlled at 2 K within a few degrees of mK in order that it will not be disturbed by change of liquid ^{4}He level in the dewar.

The output of the SQUID magnetometer was reset automatically when a magnetic flux increased over the specified value. Moreover, many breakpoints were caused by vibration of a magnetic field penetrating to the experimental space. The average number of breakpoints for one warming was about 30. To reduce these as much as possible, a lead film of 1 mm thickness was wound around the thermal shield of the still and the mixing chamber covering the entire experimental space, and welded tightly to act as a good superconducting shield. The performance of the shield was satisfactory, even though niobium and lead shields were already in use in each section.

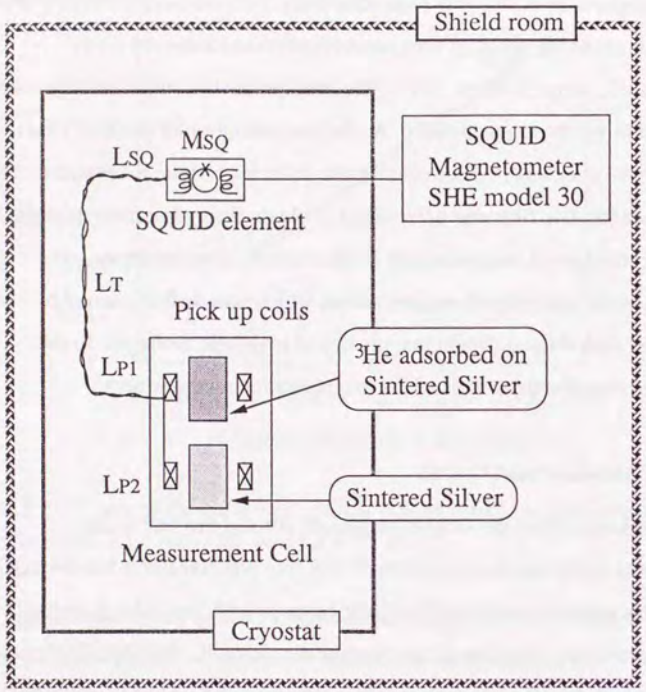

Figure 2.6 Block diagram of the magnetization measurement circuit. For denoted inductances, see text.

2.3.2 Sensitivity

The sensitivity of the circuit is calculated from the inductance of the transfer loop. As illustrated in Fig. 2.6, the transfer loop consists of the pick-up coils of each side L_{P1} and L_{P2} of 1.88 μ H, the twisted pair L_T of 0.3 μ H, the input coil of the SQUID L_{SQ} of 2μ H, and the mutual inductance M_{SQ} of 20 nH. The SQUID magnetometer has output voltage of 196 mV per one quantum flux ϕ_0 across the weak junction. The sintered silver has a cylindrical form with 8.8 mm diameter, 17.75 mm height and the surface area of 8.94 m^2.

Curie law is described as follows

$$M = N \frac{I\,(I+1)\,g^2\,\mu_N^2}{3\,k_B\,T}\,B_{ex},$$

where I is total angular momentum, g is gyromagnetic ratio multiplied by $h/2\pi$, and μ_N is nuclear magneton. Using a relation of ^{3}He nuclear magnetization $\mu = g\,\mu_N\,I$ and $I = 1/2$, the Curie law is simplified as

$$M = N\,\mu\,\frac{\mu\,B_{ex}}{2\,k_B T}.$$

Substituting the values of 4.8 mT for external field, 1.10×10^{-26} J/T for nuclear magnetic moment of ^{3}He atom and physical constants, the magnetization of the ^{3}He film with the areal density of 0.20 atoms/Å^2 is given by

$$M = \frac{7.19 \times 10^{-9}}{T}\ \mathrm{A\,m^2},$$

where T is in mK.

The magnetization is converted to the flux Φ in the transfer loop by $\Phi = 8\,S\,M$, where S is the area of pick-up coil and 8 is number of turns of the pick-up coil. The relation between the temperature and the output voltage of the SQUID is given by

$$V = \frac{1.27}{T}\ \mathrm{Volt},$$

where T is in mK.

We compare the calculation and the magnetization of ^{3}He film at 0.20 atoms/Å^2, and find that the ambiguity arising from the inductance of the transfer loop is within 5%.

2.3.3 How to Convert SQUID Output to Magnetization

The magnetization was measured as the temperature rose from 0.2 mK to 10 mK. The output voltage of the SQUID magnetometer was taken every 5 seconds. An average of the output for each 5 minutes was recorded as one magnetization data point over 4 or 5 days; in this way more than 1000 data points were obtained for each areal density. Typical SQUID output as a function of time is shown in Fig. 2.7.

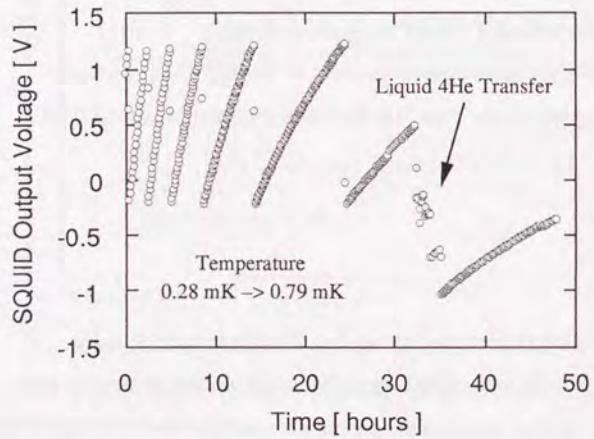

Figure 2.7 SQUID output voltage as a function of time. The magnetization data are taken in the warming process. Scattering of the data in the middle of the graph is due to a liquid ^{4}He transfer.

The breakpoints in the SQUID output were caused by auto-reset of the magnetometer or vibrations due to liquid ^{4}He transfers. The data sets of the SQUID output were connected as the magnetization to be smooth. To reduce the work of calculation, the magnetization data were picked up from 70 different typical temperatures in the form of 10 or more consecutive data sets. The data sets were connected preliminarily by a guide for the eye, and fitted to an appropriate function by the least squares residual method. Figure 2.8 shows

the typical background magnetization and that with the ^{3}He film. The difference between the two corresponds to the magnetization of ^{3}He film.

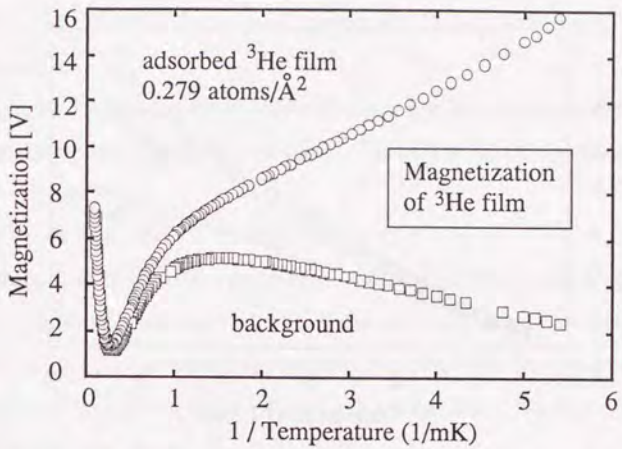

Figure 2.8 Typical magnetizations of the background and the cell with the ^{3}He film. Magnetization of the ^{3}He film is deduced from the difference between the two magnetizations.

The SQUID magnetometer detects only change in magnetic flux in the transfer loop, so that the zero point of the magnetization is not determined and the magnetization of a degenerated Fermi liquid which is independent of temperature cannot be detected. The zero point of the magnetization is determined by assuming zero at the high temperature limit. Unexpected excess magnetization was observed for temperatures higher than 2 mK, therefore we used magnetizations below 2 mK.

The data sets are fitted to various kinds of functions: Curie law, Curie-Weiss law, and second or third order of polynomial function of $1/T$. The trials of the fitting to these functions show that the magnetization below 0.20 atoms/Å^2 well obeys the Curie law and that above 0.20 atoms/Å^2 obeys the second order of polynomial function of $1/T$. Polynomial function higher than this order does not

bring a reasonable result in a physical sense, even if the residuals become less than the lower order function.

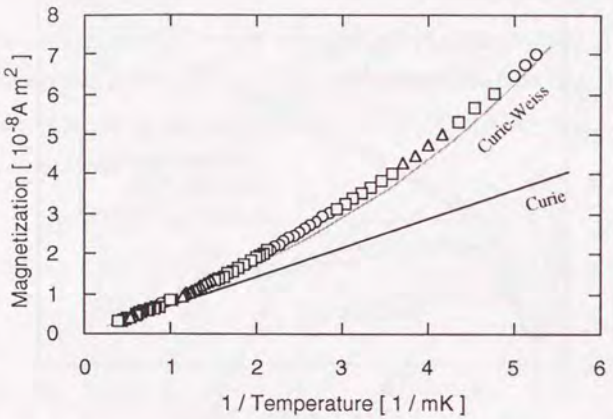

Figure 2.9 The magnetization of the ^{3}He film at 0.31 atoms/Å^2. The same symbols in the figure correspond to the same magnetization data set of the SQUID output.

2.3.4 Background Magnetization

We measured the magnetization of an empty cell as the background magnetization four times. Each background magnetization had very different temperature dependence, although common features were also recognized: for higher temperatures the background magnetization is proportional to $1/T$; the temperature dependence of the background magnetization changes around 5 and 1 mK; for lower temperatures the background magnetization is also proportional to $1/T$. These features suggest that the background magnetization consists of three different components.

The magnetization of free spin system having two energy levels is given by

$$M(T) = n\,m\,\tanh\left(mB/k_BT\right),$$

where n is number of magnetic moments, m is a magnetic moment and B is an

external field. The magnetization is nearly constant at $T<mB/k_B$, is gradually saturated around $T\sim mB/k_B$ and is proportional to $1/T$ at $T>mB/k_B$. The two inflection points are considered due to the saturation of two different magnetic moments, and $1/T$ dependence at low temperatures is considered due to paramagnetism.

We model the background magnetization as a free spin system with three different magnitudes of magnetic moments. The background magnetizations are fitted to the function

$$M(T) = c1\,\tanh(c2/T) + c3\,\tanh(c4/T) + c5/T + c6,$$

where from c1 to c6 are fitting parameters. A non-linear least squares residual method with initial condition of $c2$=1 mK and $c4$=5 mK gives the results listed in Table 2.1. A good agreement of the fitting functions with the background magnetization is obtained, and the deviation from the fitting function is less than 2% of the magnitude.

Table 2.1 Parameters of the fitting function

Number of background data	$c2$ [mK]	$c4$ [mK]
1	1.16	9.10
2	1.45	5.96
3	1.35	6.95
4	1.37	7.24

From Table 2.2 we estimate roughly $c2\sim1.4$ mK and $c4\sim7$ mK. The $c2$ and $c4$ are converted to the magnetic moment $m2$ of 0.43 μ_B and $m4$ of 2.2 μ_B using the relation $c2 = m2\,B / k_B$ and $c4 = m4\,B / k_B$.

We can take account of three different origins in the background magnetization: magnetic impurities in the silver powder, adsorbed oxygen on the surface, and difference of the magnetization of the silver powder itself.

Magnetic impurities in the silver powder, such that iron or manganese, have large magnetic moments. Iron atom has a magnetic moment of 2.2 μ_B, which value well agrees with *c2*. Oxygen diatomic molecule adsorbed on the surface has 0.17 μ_B. This value is calculated from the molar susceptibility at room temperature, and is somewhat smaller than *c4*. The magnetization of silver itself is represented by Curie law. The nuclear magnetic moment of silver is much smaller than the other two magnetic moments.

The model reasonably explains the temperature dependence of the background magnetization. To verify the model, magnetic field dependence measurement of the background magnetization is desirable.

2.4 Procedure

Knowledge of the areal density of each adsorbed layer is necessary in order to determine the number of layers. In this section the areal densities, preparation of the ^{3}He films and the experimental procedures are described.

2.4.1 Areal Density of Each Adsorbed Layer

Each adsorbed layer is compressed by the promoted atoms. The neutron experiment [8] reveals that the first layer on graphite substrate is compressed by about 4% of the density even in the incommensurate phase. Nevertheless, the density of adsorbed layers is unchanged above 0.20 atoms/Å^2. We adopt the areal density of each adsorbed layer listed in Table 2.2. These values have been used for the magnetization measurement on sintered silver and the NMR measurement on graphite.

Table 2.2 Areal densities of each layer and total layers.

Number of layers	Areal density atoms/Å^2	Total areal density atoms/Å^2
1	0.108	0.108
2	0.092	0.200
3	0.070	0.270
4	0.070	0.340

The density of subsequent numbers of layers increases by 0.070 atoms/Å^2 of the density of one liquid layer calculated from the bulk liquid density.

2.4.2 Experimental Procedure

We have done four series of magnetization measurements of ^{3}He films with two different sets of experimental cells. In the first and second series only the magnetization cell was used; in the third and fourth series the magnetization cell and buffer cell were used. The magnetization of ^{3}He films was measured for 34 different areal densities varied from 0.104 atoms/Å^2 up to 0.548 atoms/Å^2 in steps of about 0.02 atoms/Å^2, and 4.5 atoms/Å^2. These coverages correspond to the number of atomic layers from 0.96 layers up to 7.0 layers in steps of a quarter atomic layer, and 65 layers.

The measurement procedure was as follows: The magnetization of the empty cell was measured first as the background magnetization; an appropriate amount of ^{3}He gas was introduced to the cells and the magnetization with the ^{3}He film was measured; magnetization of the ^{3}He film alone was obtained from the difference between the magnetization with the film and the background magnetization. This procedure was repeated adding the ^{3}He gas. The magnetizations were measured under warming without artificial heating.

To prevent the capillary condensation of the ^{3}He gas, the inlet capillary to the cells warmed to 4 K. The magnetization measurement was completed at 10

mK, and the pumping of the dilution refrigerator and 1 K plate was stopped by opening the heat switch. After a few hours the whole capillary was sufficiently warmed with the experimental cells remaining in several hundred mK, and an appropriate amount of ^{3}He gas was introduced. Then the experimental cells were kept at 4.2 K over 24 hours to form a uniform ^{3}He film and an annealing of the film. After the annealing, the film was cooled down below 0.2 mK by the nuclear refrigerator. The experimental cells stayed below 0.2 mK for about one day. The magnetization relaxed completely within a few hours after the demagnetization had finished, therefore the ^{3}He film should be completely thermal equilibrium in the warming. Figure 2.10 shows typical temperatures of the nuclear stage as a function of time. At least ten days were required for a single magnetization measurement.

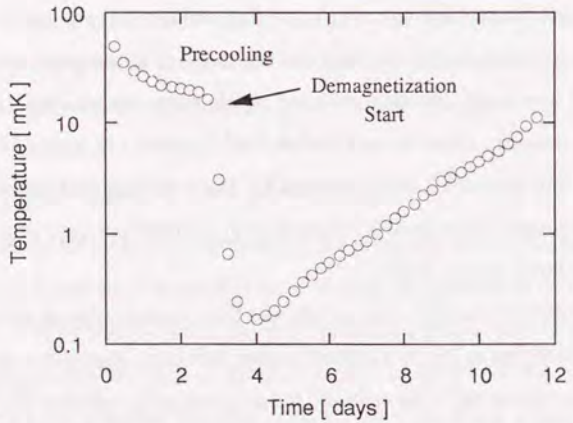

Figure 2.10 Typical temperature of the nuclear stage as a function of time. The demagnetization starts after three days precooling. The nuclear stage is cooled down to 0.17 mK or less.

3. Results

In this section we describe details of the experimental results that: 1) The ferromagnetic interaction appears above 0.20 atoms/Å^2; 2) The isotherm of the magnetization at the lowest temperature has four peaks at 0.23, 0.29, 0.35, and 0.41 atoms/Å^2; 3) The Curie constant increases in proportion to the coverage below 0.20 atoms/Å^2, and becomes constant above 0.20 atoms/Å^2; 4) The exchange constant begins to appear above 0.20 atoms/Å^2 and increases as the coverage increases, and saturates above 0.30 atoms/Å^2; 5) The exchange constant has four peaks at 0.23, 0.29, 0.35, and 0.41 atoms/Å^2, which appear with the same interval of 0.06 atoms/Å^2.

3.1 Magnetizations

The magnetization of ^{3}He films adsorbed on sintered silver is measured for 34 coverages ranging from 0.10 atoms/Å^2 to 0.54 atoms/Å^2 in steps of about 0.02 atoms/Å^2 and 4.5 atoms/Å^2. These coverages correspond to the number of layers from a monolayer to 7 layers in steps of about a quarter layer and 65 layers.

The temperature dependence of the ^{3}He films shows that up to 0.20 atoms/Å^2 the magnetization obeys well Curie law, and above 0.20 atoms/Å^2 the magnetization increases with an upward curvature which represents the ferromagnetic interaction in the ^{3}He film. Figure 3.1 shows the temperature dependence of the magnetization for typical coverages.

Figure 3.2 shows the isotherms of magnetization at 0.2 mK and 0.5 mK. The isotherm at 0.5 mK shows that the magnetization increases as the coverage increases up to 0.27 atoms/Å^2, and becomes almost constant above that. As the temperature decreases to 0.2 mK, the isotherm reveals a unique structure. From 0.10 atoms/Å^2 to 0.20 atoms/Å^2 the magnetization increases in proportion to

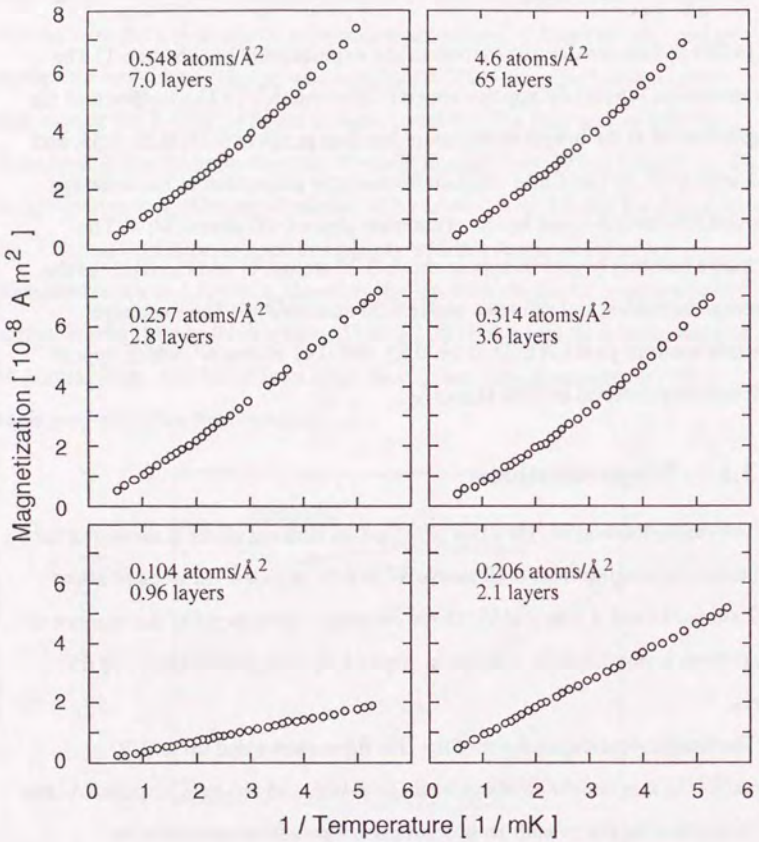

Figure 3.1 Magnetization for typical coverages of ^{3}He films.

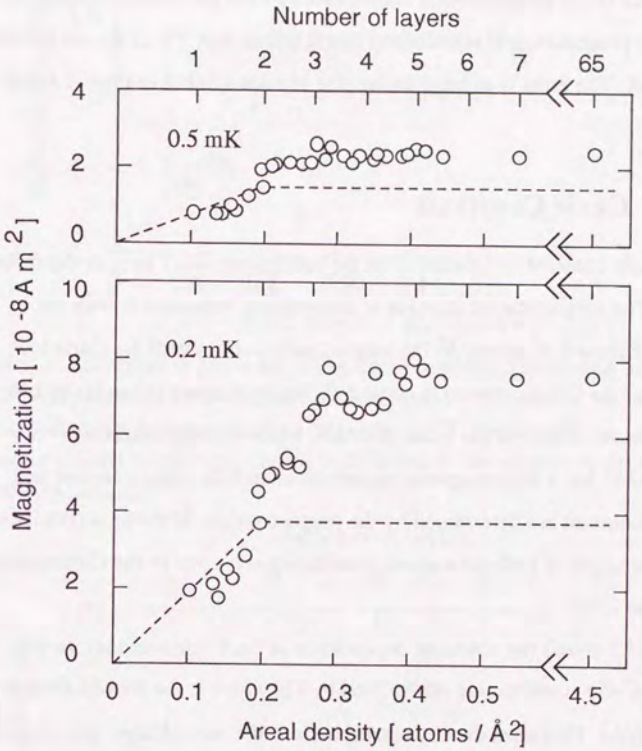

Figure 3.2 Isotherm of the magnetization as a function of coverage. Dashed lines indicate magnetization of free spins (below 0.20 atoms/Å^2) and Fermi-degenerated liquid (above 0.20 atoms/Å^2). Above 0.20 atoms/Å^2 the ferromagnetic interaction comes out, and the magnetization varies with oscillation as the coverage increases.

the coverage, and varies with oscillation with four peaks above 0.20 atoms/Å^2 as the coverage increases.

The error of the magnetization comes mainly from the connection and the subtraction procedure, and is estimated that it is less than 5% of the magnitude below 2 mK. The error is as large as the size of each symbol in Figs. 3.1 and 3.2.

3.2 Curie Constants

The Curie constant is deduced from the coefficient of $1/T$ term in the fitting function. The magnetization changes in temperature dependence with the coverage. Below 0.20 atoms/Å^2 the magnetization obeys well the Curie law. The error of the Curie constant is about 5 %, so the magnetization is used for the determination only of the Curie constant, while the magnetization above 0.20 atoms/Å^2 has a ferromagnetic contribution, and the Curie constant and exchange constant are determined by the magnetization. With the difficulty of the determination of both parameters simultaneously, error of the Curie constant increases to 20 %.

Figure 3.3 shows the coverage dependence of the Curie constant. In the figure the Curie constants are normalized by C_0, which is the free spin value of 0.20 atoms/Å^2. This areal density corresponds to the second layer completion. From 0.10 atom/Å^2 to 0.20 atoms/Å^2 the Curie constant is smaller than the free spin value. At 0.20 atoms/Å^2 Curie constant agrees well with free spin value, and above that it becomes $(1.2 \pm 0.2)\ C_0$, which corresponds to 2.6 ± 0.6 layers.

3.3 Exchange Constants

The ferromagnetic tendency appears in the magnetization above 0.20 atoms/Å^2. The ring exchange theory [11] estimated that in the first layer the exchange interaction is strongly suppressed by its high density to be of the order

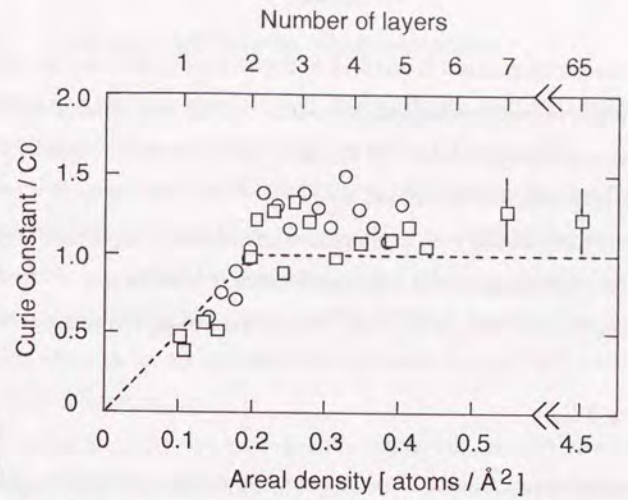

Figure 3.3 Coverage dependence of the Curie constant. The dashed line shows the dependence of the two solid layers model. ○, results of measurement with the magnetization cell alone; □, results with the magnetization and buffer cells. Below 0.20 atoms/Å^2 the error is as large as symbol size indicates.

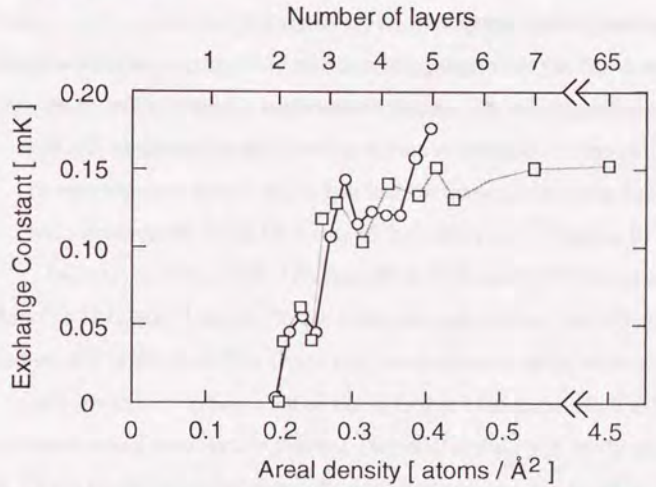

Figure 3.4 Coverage dependence of the exchange constant showing four prominent peaks. ○, results of measurement with the magnetization cell alone; □, results with the magnetization and buffer cells.

of μK. The exchange constant is deduced with assumptions that only the second layer contributes to the ferromagnetic interaction and the areal density of the second layer is unchanged above 0.20 atoms/Å^2. The areal density of 0.092 atoms/Å^2 is used as that of the second layer.

The leading and second term of a high temperature series expansion of the 2D Heisenberg ferromagnet with a triangular lattice is used for the magnetization from 0.2 mK up to 2 mK. The 2D Heisenberg ferromagnet is given by

$$M = \frac{C}{T} + \frac{3CJ}{T^2},$$

M is the magnetization, C is the Curie constant of only the second layer, and J/k_B is the exchange constant. The magnetization is determined by the fitting of the SQUID output to the second order polynomial function of $1/T$. J/k_B is obtained from the coefficient of $1/T^2$ of the fitting function divided by $3C$. As the Curie constant of the second layer is unchanged, the exchange interaction has the same coverage dependence of the magnetization.

Figure 3.4 shows the coverage dependence of the ferromagnetic exchange constants, where circles and squares represent the results of different sequences of measurements. A different sequence refers to the difference in ^{3}He film sample. For common features, we find that the exchange constant appears above 0.20 atoms/Å^2, has peaks at 0.23 atoms/Å^2 and 0.29 atoms/Å^2, and increases from 0.38 atoms/Å^2 to 0.40 atoms/Å^2. The exchange constant represented by the squares also has peaks at 0.35 atoms/Å^2 and 0.41 atoms/Å^2. Thus the results of the two sequences agree well with each other. The exchange constant of both sequences has four peaks as the coverage increases. The magnitude of the first peak is 0.06 mK, and that of following peaks about 0.15 mK. The interval between these peaks is almost constant at 0.06 atoms/Å^2. For higher coverages, the exchange constant J/k_B becomes 0.15 mK.

3.4 Unexpected Excess Magnetization

Unexpected excess magnetization is observed in the magnetization for temperatures above 3 mK and for coverages above 0.35 atoms/Å^2.

Typical temperature dependences of the magnetization at the coverage, 0.414, 0.548, and 4.5 atoms/Å^2 are shown in Fig 3.5. These coverages correspond to 3, 5, and 63 liquid layers. Below 2 mK the magnetizations well obey the 2D Heisenberg ferromagnet, and it decreases as the temperature increases, although the magnetization has minimum around 3 mK, and increases as the temperature increases.

The excess magnetization is obtained by subtracting the 2D Heisenberg ferromagnet from the magnetization. Figure 3.6 shows the excess magnetization of typical coverages. It appears in a thick ^{3}He film with more than three liquid layers, and increases in proportion to liquid layers up to five layers, while the excess magnetization of 63 liquid layers is a little larger than that of 5 liquid layers, but not proportional to the liquid layer thickness. The temperature dependence of the excess magnetization is almost proportional to T, and seems to saturate around 10 mK. Above 2 mK the magnetization of the ^{3}He film becomes small. The estimation of the error is about 50 %, although we believe that excess magnetization exists.

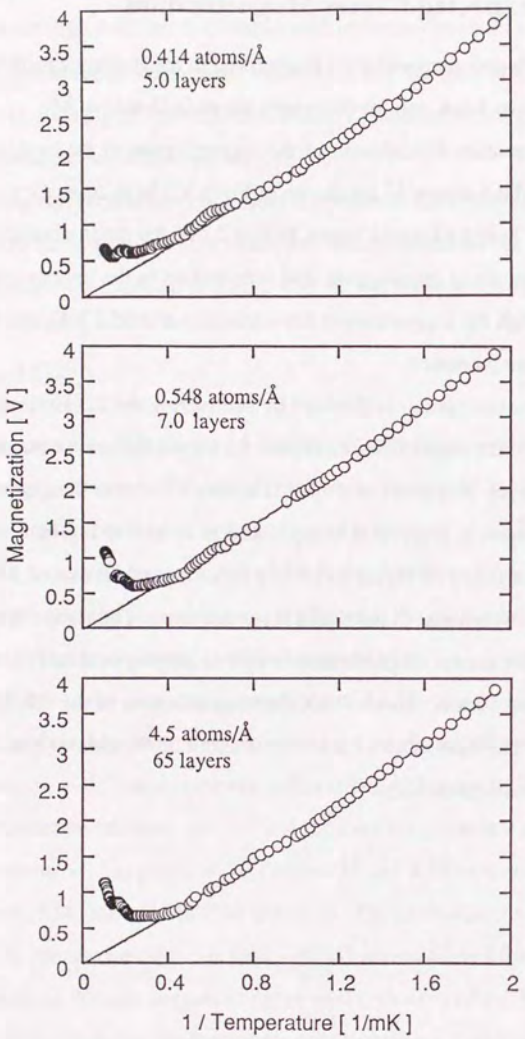

Figure 3.5 Typical temperature dependence of the magnetization for higher coverages. The solid line represents 2D Heisenberg ferromagnet. The magnetization deviates from the solid line above 2 mK. For coverages above 0.548 atoms/Å the excess magnetization is more outstanding.

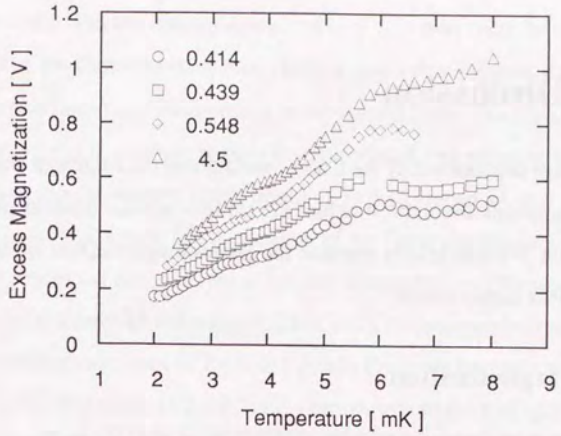

Figure 3.6 Excess magnetization as a function of temperature. The excess magnetization saturates as the temperature rises.

4. Discussion

The coverage dependence of the Curie constant and the exchange constant provides informations about the structure of ^{3}He film and the mechanism of ferromagnetism. We will briefly mention the excess magnetization which appears at higher temperatures.

4.1 Magnetization

The temperature dependence of the magnetization changes from paramagnetism to ferromagnetism as the coverage increases. Above 0.20 atoms/Å^2 the ferromagnetic contribution appears as an upward curvature in the magnetization, although a spontaneous magnetization does not appear even at the lowest temperatures. In the previous magnetization measurement of the ^{3}He film adsorbed on sintered silver using the field cooling method no spontaneous magnetization was observed even at 0.15 mK with zero magnetic field [29]. This feature is one of those characteristic of the 2D Heisenberg ferromagnet. The temperature dependence of the increase of the magnetization is not as strong as the Curie-Weiss law, but is well represented by 2D Heisenberg ferromagnet, thus making this ferromagnet a more suitable model than the Curie-Weiss law for temperatures between 0.2 and 2 mK. To determine the character of the ferromagnetism of the ^{3}He film from the temperature dependence, magnetization measurements below 0.15 mK are desirable.

4.2 Curie Constant

Below 0.20 atoms/Å^2, we obtain the following results: The magnetization well obeys Curie law, the Curie constant is smaller than the free spin value, and at 0.2 atoms/Å^2 the Curie constant agrees well with the free spin value. Since it

obeys the Curie law, the magnetization has only free spin contribution. Reduction of the Curie constant from the free spin value suggests the coexistence of liquid and solid phases in the second layer. The coverage dependence of Curie constant reveals that introduced ^{3}He atoms to the second layer behave as a degenerate Fermi liquid up to 0.15 atoms/Å^2, and solidify gradually up to 0.20 atoms/Å^2. Agreement of the Curie constant and the free spin value causes the second layer to solidify completely at 0.20 atoms/Å^2.

Above 0.20 atoms/Å^2 the magnetization has a ferromagnetic contribution, the Curie constant becomes $(1.2 \pm 0.2)\, C_0$, and C_0 is the free spin value of 0.20 atoms/Å^2. The value $(1.2 \pm 0.2)\, C_0$ corresponds to the free spin amount of 2.6 ± 0.6 atomic layers. Assuming a layer by layer configuration, we conclude that at least the first and second layers exist as solid on the sintered silver substrate. Other experiments with the ^{3}He films on graphite substrate also show that the second layer solidifies above 0.20 atoms/Å^2. The NMR measurement [6] shows that the magnetization of the ^{3}He film at 0.233 atoms/Å^2 has the Curie constant of C_0. The heat capacity measurement [4] indicates that the second layer solidifies at 0.186 atoms/Å^2.

^{3}He film adsorbed on sintered silver [10] shows a large temperature independent heat capacity above 0.16 atoms/Å^2. A similar anomalous large heat capacity has been observed as an excess heat capacity in the measurements of bcc solid ^{3}He. This excess heat capacity appears for temperatures below 300 mK, and depends on the surface area of heat exchangers and the quality of solid ^{3}He. In recent precise measurement [30], the excess heat capacity was deduced as the difference between the heat capacity and the converted value from the pressure of constant volume measured simultaneously. Figure 4.1 shows the temperature dependence of the excess heat capacity which seems to be constant from 7 mK to 50 mK, and has an average of 2.6×10^{-2} J/Kmol. With the surface area of 58 m^2 and sample volume of 2.42 cm^3 at molar volume of 24.23 cm^3/mol, the excess heat capacity equals 0.32 k_B per ^{3}He atom in the second

layer. This suggests that the large temperature independent heat capacity on sintered silver does not conflict with the solidification of the second layer, and that heat capacity is likely related to the defects or imperfections in the second layer.

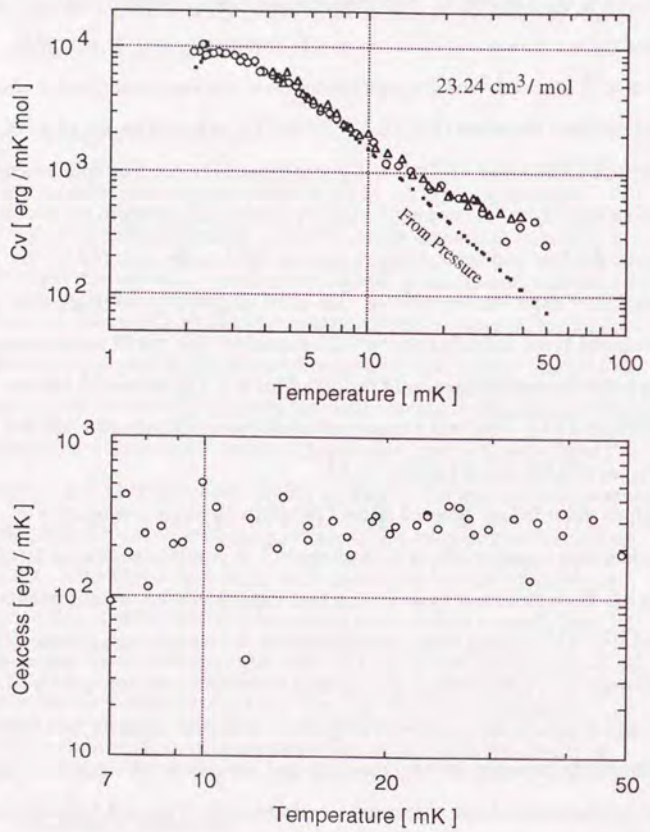

Figure 4.1 Excess heat capacity appeared in the heat capacity measurement of bcc solid ^{3}He [30]. Upper graph shows the heat capacity and the converted value from the pressure measurement, while the lower graph shows the excess heat capacity.

4.3 Exchange Constant

The first peak at 0.23 atoms/Å^2 is commonly observed on both sintered silver and graphite substrates, but the magnitude of the exchange constant differs. The value at 0.23 atoms/Å^2 on each of the two substrates is listed in Table 4.1. On graphite substrate, the exchange constants obtained from the magnetization and the heat capacity measurements agree well, while on sintered silver substrate that deduced from the magnetization measurement is one third that from the heat capacity measurement.

Table 4.1 Exchange interaction of ^{3}He film at 0.23 atoms/Å^2.

	Magnetization	Heat capacity
Sintered silver	0.06 mK	0.17 mK
Graphite	2.1 mK	1.7 mK

Two possible explanations may account for the difference of the exchange constant on sintered silver: one is the large heat capacity and the other is the even particle exchange process in the second layer.

The heat capacity has a large temperature independent heat capacity above 0.16 atoms/Å^2. If this large heat capacity is due to imperfections or defects in the second layer, it can be subtracted from the total heat capacity and the exchange constant then decreases to 0.09 mK or less. This value is fairly consistent with that of the magnetization result.

The low density of the second layer implies that two particle or four particle exchange may not be negligible. These even particle exchanges result in antiferromagnetism, and decrease the magnitude of the ferromagnetism, but increase the exchange contribution to the heat capacity.

The exchange constant at the thickest coverage of 4.5 atoms/Å^2 is almost 0.15 mK. This ^{3}He film has a thickness of about 200 Å, which is thought a bulk

liquid. The exchange constant of thick ^{3}He films or with bulk liquid is as follows: that deduced from the heat capacity of the ^{3}He film at 0.4 atoms/Å^2 on sintered silver is 0.14 mK [10]; on graphite the exchange constant acquired from the heat capacity measurement decreases toward 0.14 mK for higher coverage [4].

In the previous studies at higher temperatures, the ferromagnetic interaction was obtained as Weiss temperature θ. The relation between the exchange constant J/k_B and Weiss temperature θ is given by $\theta=3J/k_B$. Weiss temperature of 0.4 mK is obtained from the magnetization measurement on sintered silver [9]. On graphite Weiss temperature deduced from the NMR measurement decreases toward 0.5 mK for higher coverage [5]. Moreover, on various substrates Weiss temperature θ is around 0.5 mK.

The exchange constant with bulk liquid ^{3}He results in about 0.15 mK on various substrates, and seems to be independent of the substrate. This suggests that the exchange constant is also independent of solid quality of the second layer, and that the indirect exchange process via liquid ^{3}He is favorable for the ^{3}He film with the bulk liquid.

The exchange constant of the ^{3}He film has four peaks as the coverage increases. The first appears at 0.23 atoms/Å^2, and following peaks appear at 0.29, 0.35, and 0.41 atoms/Å^2. Each locates with almost the same interval of 0.06 atoms/Å^2.

On graphite substrate very recent heat capacity measurement [31] revealed a small peak of the exchange constant at 0.07 atoms/Å^2; this peak and a commonly observed large peak at 0.23 atoms/Å^2 are considered due to the direct exchange interaction in the first and second layers, respectively. In the present study we observed three peaks larger than the first peak above 0.23 atoms/Å^2. These cannot be explained by the direct exchange interaction in the second layer, and are considered to be a result of the indirect exchange interaction.

The indirect exchange via the 2D degenerated liquid layer [14] predicts that the exchange constant has several peaks as the coverage increases which appear at the half-filled state of each liquid layer. In studies on liquid ^{3}He thin films regarded as an ideal 2D degenerated Fermi liquid, the density of one liquid layer was found to be smaller than 0.07 atoms/Å^2, as calculated from the density of bulk liquid ^{3}He. The NMR measurement [32] showed step-like doublings of the magnetization at 0.05 atoms/Å^2 and 0.10 atoms/Å^2, which were ascribable to the promotion to higher energy levels. The interval of these steps represents the density of one adsorbed liquid layer. The heat capacity measurement [4] shows that the promotion to the fourth liquid layer happens when the third liquid layer density is 0.045 atoms/Å^2.

Figure 4.2 shows the exchange constant replotted with a single liquid layer thickness of 0.060 atoms/Å^2. The multipeak structure for higher coverages agrees well with the prediction of the indirect exchange interaction theory.

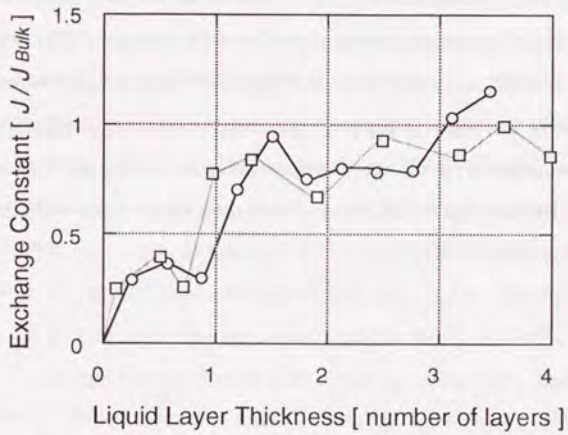

Figure 4.2 The exchange constant replotted with one liquid layer thickness of 0.060 atoms/Å^2. ○, results of measurement with the magnetization cell alone; □, results with the magnetization and buffer cells. The peaks of the exchange constant of both measurements agree well, and are placed at the half filled states of each liquid layer.

4.4 Excess Magnetization

The origin of this excess magnetization is not understood. It is extremely large compared with the free spin magnetization of the first and second layers, 5 times that of the two solid layers at 10 mK.

It is a very mysterious temperature dependence $dM/dT > 0$. The Fermi liquid theory [33] predicts that the magnetization of bulk liquid ^{3}He has a maximum around 30 mK and temperature dependence $dM/dT > 0$, although the difference between the maximum and zero temperature magnetizations is less than 1% of that value. The dependence of $dM/dT > 0$ is observed in the study of 2D Fermi liquid [32], and the phenomenon is considered to be the thermal excitation to the upper energy level in 2D Fermi liquid. The increment of the magnetization is also less than that of bulk liquid. The excess magnetization is not explained by the magnetization of the liquid layer because of its large magnitude.

The excess magnetization is not proportional to the amount of liquid ^{3}He; it begins to appear in the magnetization of the ^{3}He film with more than 3 liquid layers, and does not greatly change in that with more than 5 liquid layers. In magnetization measurement of liquid ^{3}He with sintered silver powder [34] the excess magnetization is not observed under a pressure of 1.22 or 29.51 bars. This behavior implies that the excess magnetization likely is probably related to the free surface of liquid ^{3}He.

5. Conclusion

In this study, we measured the magnetization of adsorbed ^{3}He films for areal densities from 0.104 atoms/Å^2 up to 0.548 atoms/Å^2, and 4.5 atoms/Å^2, and for temperatures between 0.2 mK and 10 mK. The magnetization was measured by a SQUID magnetometer with an external field of 4.8 mT.

The followings results were obtained:

1) The temperature dependence of the magnetization changes at 0.20 atoms/Å^2. The areal density 0.20 atoms/Å^2 corresponds to the second layer completion. Below 0.20 atoms/Å^2 the magnetization well obeys Curie law, while above that the ferromagnetic interaction appears in the magnetization, but a spontaneous magnetization does not appear even below 0.2 mK. The magnetization obeys 2D Heisenberg ferromagnet model rather than Curie-Weiss law. The isotherm of the magnetizations as a function of coverage at 0.2 mK has four peaks at 0.23, 0.29, 0.35, and 0.41 atoms/Å^2.
2) The Curie constant is deduced from the coefficient of $1/T$ term of the fitting function to the magnetization. Below 0.20 atoms/Å^2 the Curie constant is smaller than the free spin value. At 0.20 atoms/Å^2 Curie constant agrees well with free spin value. In this region, the error of the Curie constant is about 5 %. The small Curie constant suggests the coexistence of liquid and solid in the second layer. The agreement with the free spin value at 0.20 atoms/Å^2 suggests that the second layer solidifies completely. Above 0.20 atoms/Å^2 the Curie constant becomes $(1.2 \pm 0.2)\ C_0$, where C_0 is the free spin value of 0.20 atoms/Å^2. This Curie constant corresponds to the free spin value of 2.6 ± 0.6 layers. Because of the difficulty of determining the Curie constant and the exchange constant simultaneously, the error of the former

increases to 20 %, but this Curie constant shows that at least the first and second layers solidify above 0.20 atoms/Å^2.

3) The exchange constant is deduced from the magnetization on the following assumptions: Only the second layer contributes to the ferromagnetism; Curie constant of the second layer above 0.20 atoms/Å^2 is constant when more ^{3}He atoms are promoted to liquid layers above the second layers. The exchange constant begins to appear at 0.20 atoms/Å^2 and increases as the coverage increases; moreover, it has four peaks at 0.23, 0.29, 0.35, and 0.41 atoms/Å^2. At the first peak the exchange constant J/k_B is 0.06 mK, and at following peaks J/k_B is about 0.15 mK. These peaks appear with the same interval of 0.06 atoms/Å^2, which is nearly equal to the areal density of a single liquid layer. The multipeak structure of the exchange constant in the coverage dependence implies that the exchange process dynamically changes as the coverage increases and is dependent on the number of liquid layers.

A number of questions still remain. On sintered silver substrate the second layer has a free spin magnetization, while it has a significantly large temperature independent heat capacity. The excess magnetization has a mysterious temperature dependence and an anomalous magnitude. These will be future areas of interest in which we hope to further our knowledge of this complex interrelationship.

References

1 A. I. Ahonen, T. Kodama, M. Krusius, M. A. Paalanen, R. C. Richardson, W. Schoepe and Y. Takano; J. Phys., **C9**, 1665 (1976).

2 R. C. Richardson; Physica (Amsterdam) **126B**, 298 (1984).

3 D. W. Brewer; in "Physics of Liquid and Solid Helium, Part 2" edited by K. H. Bennemann and J. B. Ketterson, Wiley, New York (1978).

4 D. S. Greywall; Phys. Rev. B, **41**, 1842 (1990).

5 H. Franco, R. Rapp and H. Godfrin; Phys. Rev. Lett., **57**, 1161 (1986).

6 H. Godfrin, R. R. Ruel and D. D. Osheroff; Phys. Rev. Lett., **60**, 305 (1988).

7 H. J. Lauter, H. D. Schildberg, H. Godfrin, H. Wiechert and R. Haensel; Can. J. Phys. **65**, 1435 (1986).

8 H. J. Lauter, H. Godfrin, V. L. P. Frank and H. P. Schildberg; Physica B, **165** & **166**, 597 (1990).

9 Y. Okuda, A. J. Ikushima and H. Kojima; Phys. Rev. Lett., **54**, 130 (1985). From the precise measurement of the surface area of the experimental cell, the surface area should be revised from 5.15 m^2 to 8.94 m^2. The number of layers in the results of the previous paper should be changed to about half value.

10 D. S. Greywall and P. A. Busch; Phys. Rev. Lett., **60**, 1860 (1988).

11 M. Roger and J. M. Delrieu; Jpn .J. Appl .Phys., **26**, 267 (1987).

12 T. Mamiya, H. Yano, H. Kondo, T. Suzuki, T. Kato, Y. Minamiide, Y. Miura and S. Inoue; Physica B, **165** & **166**, 837 (1990).

13 H. Jichu and Y. Kuroda; Prog. Theor. Phys., **67**, 715 (1982); **69**, 1358 (1983).

14 R. A. Guyer; Phys. Rev. Lett., **64**, 1919 (1990).

15 G. A. Baker Jr., H. E. Gilbert, J. Eve and G. S. Rushbrooke; Phys. Lett., **25A**, 207 (1967).

16 N. D. Mermin and H. Wagner; Phys. Rev. Lett., **17**, 1133 (1966).

17 Y. Okuda and A. J. Ikushima; Jpn. J. Appl. Phys., **25**, 750 (1986).

18 S. H. E. Corp., U. S. A., model DPR 420.

19 N. E. C. Corp., Japan, model PC-9801E.

20 Y. Jinzaki, Y. Okuda and A. J. Ikushima; Cryogenics **23**, 321 (1983).

21 N. I. S. T., U. S. A., model SMR-768, superconducting fixed points device from 200 mK to 15 mK.

22 The annealing treatment was done by Mr. K. Sakayori in Ishimoto Lab of I. S. S. P.
23 Vacuum Metallurgical Corp., Tokyo, Japan.
24 S. Brunauer, P. H. Emmet and E. Teller; J. Am. Chem. Soc., **60**, 309 (1938).
25 Datametrics®, U. S. A., model 600A-100T.
26 Setra Systems INC., U. S. A., model 204.
27 S. J. Gregg and K. S. W. Sing; "Adsorption, Surface Area and Porosity", 2nd ed., Academic Press, London (1982).
28 S. H. E. Corp., U.S.A., model system 30.
29 Y. Okuda, A. Fukushima and A. J. Ikushima; Jpn. J. Appl. Phys. **26**, 269 (1987).
30 H. Fukuyama, Y. Miwa, A. Sawada and Y. Masuda; J. Phys. Soc. Jpn. **53**, 916 (1984).
31 D. Greywall and P. Busch; Phys. Rev. Lett., **65**, 2788 (1990).
32 R. H. Higley, D. T. Sprague and R. B. Hallock; Phys. Rev. Lett., **63**, 2570 (1989).
33 S. Misawa; Phys. Lett., **32A**, 153; **32A**, 541 (1970).
34 T. Hata, S. Yamasaki, T. Kodama and T. Shigi; J. Low Temp. Phys., **71**, 193 (1988).